

Optimal control of DC motor using leader-based Harris Hawks optimization algorithm



Shehu Lukman Ayinla^{a,b}, Temitope Ibrahim Amosa^{a,*}, Oladimeji Ibrahim^c, Md. Siddikur Rahman^a, Abdulrahman Abdullah Bahashwan^a, Mohammad Golam Mostafa^a, Abdulrahman Olalekan Yusuf^b

^a Department of Electrical and Electronics Engineering, Universiti Teknologi PETRONAS, Bandar Seri Iskandar, Tronoh, Perak 32610, Malaysia

^b Department of Computer Engineering, University of Ilorin, Ilorin 240103, Nigeria

^c Department of Electrical and Electronics Engineering, University of Ilorin, Ilorin 240103, Nigeria

ARTICLE INFO

Keywords:
 DC motor
 Leader Harris Hawks optimization (LHHO)
 FOPID controller
 ITAE
 Meta-heuristic algorithms

ABSTRACT

Direct Current (DC) motor is considered a very critical component of various industrial drive equipment. This is due to their unique advantages including reasonable cost, speed-torque characteristics, ease of control, etc. While most DC motor drive applications often employ PID controllers to regulate the speed of the machine, selecting the optimal design parameters for the controllers used in these applications often posed a serious challenge. Moreover, as the complexity of the industrial process increases, the need for precise speed and position tracking becomes necessary. This current study proposes a novel Leader-based Harris Hawks Optimization (LHHO) algorithm for the design of Proportional-Integral-Derivative (PID) and Fractional Order Proportional-Integral-Derivative (FOPID) controllers to achieve optimal speed regulation of DC motors. The LHHO algorithm is an innovative meta-heuristic algorithm that draw inspiration from the cooperative hunting behavior and leadership prowess of the Harris Hawks called the “seven pounds”. While several error functions were tested in this study, the integral of time multiplied absolute error (ITAE) has been adopted as the error function for obtaining the parameters of PID and FOPID controllers using the LHHO algorithm. Through quantitative evaluations and comparisons with existing techniques, the proposed controllers (LHHO-PID and LHHO-FOPID) have revealed significant improvements in key performance metrics, including rise time, settling time, and maximum overshoot during transient periods when ITAE is used as the error function. Furthermore, the stability response and robustness analyses were carried out by varying the parameters of the DC motor under eight scenarios, which confirmed competitive performance in system response and transient behavior.

1. Introduction

Direct Current (DC) motors remain the most preferred choice for a wide range of high-performance motion control applications. These motors are particularly well-suited for low-power and highly precise servo applications due to their attractive features such as cost-effectiveness, favorable speed-torque characteristics, and ease of control [1–3]. These distinctive advantages place them as the preferred choice across various industrial sectors, where precise speed control and cost efficiency are of paramount importance. Consequently, position control of DC motor has attracted substantial research attention over the years, and several techniques have been proposed [4–6]. In the context of industrial applications, traditional motor controls employ a feedback

control structure to regulate the operation of a plant and maintain desired output characteristics in relation to the reference signal. Within a feedback control system, a representative parameter is measured to capture the system’s output. Any detected variations in this parameter are then leveraged to modify the plant’s operational characteristics, with the goal of regulating the system and ensuring that the output meets the desired specifications. The primary purposes of a feedback control system revolve around mitigating the influence of disturbances on the system’s output and minimizing the sensitivity of the closed-loop response to fluctuations in plant parameters [7]. This system involves an actuator that modifies the signal within a continuous feedback loop via a controller.

Proportional-Integral-Derivative (PID) controllers are a popular

* Corresponding author.

E-mail address: temitope_21002075@utp.edu.my (T.I. Amosa).

choice for speed and position control of DC motors owing to their notable attributes such as simplicity, reliability, transparency, high efficiency, and robustness [8,9]. These controllers have gained widespread acceptance for control in process and automation industries globally. Various modes of the PID control system, including proportional only (P-mode), proportional and integral (PI-mode), proportional and derivative (PD-mode), as well as proportional, integral and derivative (PID-mode), can be implemented to meet the specific needs of the various processes [8,10]. While integer order PID controllers provide robust and fairly good performance, the selection of their design parameters yields suboptimal results. Another controller closely related to the conventional PID is the Tilt Integral Derivative (TID) controller. In this controller, the proportional coefficient is substituted with a component that exhibits a transfer function represented by $1/s^{-n}$. This component, known as the tilt, introduces a frequency-dependent feedback gain that is shaped or tilted relative to the proportional coefficient [11,12].

In control engineering, the accurate modeling of system dynamics plays a crucial role in determining the overall performance of any control strategy. It has been observed that several real-world dynamic systems can be better characterized using a non-integer order dynamic model based on fractional calculus, as evidenced by recent studies. Due to the availability of various approximation methods for fractional differentiation and integration, the significance of fractional order calculus in controller design is becoming increasingly apparent. Fractional Order PID (FOPID) is an improved version of the traditional PID controller, utilizing fractional derivative-integral calculus [4,13]. This controller consists of two additional parameters: the order of fractional integration (λ) and the order of fractional derivative (μ), in addition to the gains of the conventional PID. By introducing this expansion to the conventional PID, the controller becomes more robust and flexible [14]. Studies have shown that non-integer order controllers provide more flexibility in adjusting gain and phase characteristics for integer order plants compared to integer order controllers. These characteristics make Fractional Order controller a valuable tool in creating robust control systems with fewer controller parameters to tune [15].

Due to the increasing complexity of industrial processes, tuning controller parameters has become a challenging task [16]. While classical integer-order PID controller has three parameters to tune, FOPID controller has additional two tuneable parameters. The larger number of parameters in FOPID makes them more challenging to tune. The efficacy of fractional order controllers in practical applications largely depends on their tuning methodologies. Thus, without proper tuning, the performance of these controllers can suffer significantly, particularly when faced with conflicting design specifications [17]. Mainly, tuning methods can be categorized into numerical, analytical, and rule-based [18,19]. Heuristic based tuning methods fall into the category of numerical approach and have been widely used by many researchers in the literature [20–28]. These algorithms are commonly used to tune controller parameters for real-world applications such as DC motor speed control, automatic voltage regulation, functional electrical simulation system, etc. These applications serve as a testbed to evaluate the performance of meta-heuristic optimization algorithms. While various meta-heuristic optimization algorithms such as CPSO [29], GWO [30], PSO [6], GA [31], IWO [32], SFS [33], IGWO [34], ASO [35], ISMA [36, 37], etc., have been employed to tune the gain parameters of PID and FOPID controllers in DC motor speed regulation applications, studies that explored the unique cooperative behavior and chasing pattern in Harris Hawks Optimizer (HHO) and its improved version (Leaders Harris Hawks Optimizer) for DC motor speed control remain limited.

To leverage the improvement brought to the exploration and exploitation of optimal solution space by LHHO's adaptive chasing pattern and unique cooperative behavior, this current work proposed an LHHO-based PID and FOPID controllers for speed control of DC motor. The parameters of these controllers are optimally tuned using Harris Hawk-based algorithms with various objective functions. A critical

stability as well as the robustness analyses of the proposed controllers was carried out with reasonable variations in the parameters of the plant. The outcomes of proposed control schemes were effectively evaluated in comparison with established methodologies documented in the existing literature. The unique contributions of the approaches suggested in this paper can be summarized in threefold:

- This study proposes a novel application of Leaders Harris Hawk Optimization (LHHO) algorithm for optimal parameters tuning of PID and FOPID controllers in DC motor speed regulation.
- The effectiveness of the optimally designed controllers (LHHO-PID and LHHO-FOPID) was rigorously verified in relation to performance criteria and convergence profiles.
- The proposed LHHO-PID and LHHO-FOPID controllers demonstrated better robustness against system model uncertainty, thereby improving performance as compared to other common controllers [6,34,35,38].

The rest of this paper is organized into the following sections: Section 2 provides a review of the related literature, while Section 3 outlines the details of DC motor, including its model and design requirements. In Section 4, the proposed Leader Harris Hawk Optimization (LHHO) algorithm is presented, along with a discussion of the fundamental concepts of PID and FOPID controllers in Section 5. The proposed system is described in Section 6, and the simulation results are discussed in Section 7. Finally, Section 8 concludes the study.

2.0. Related work

Several studies have been identified in the literature that employ diverse meta-heuristics optimization algorithms to tune the parameters of the control system. In the study described in [4], ASO-PID, ASO-FOPID, and ChASO-FOPID controllers were developed using objective functions of ITAE and Integral Time Multiplied Square Error (ITSE) for the control of DC motor. The performance of the proposed controllers were compared with GWO-FOPID [16], GWO-PID [16], IWO-PID [39], and SFS-PID [40] controllers. The findings indicate that ASO-FOPID and ChASO-FOPID controllers exhibit better performance compared to the existing approaches. A study conducted in [16] aimed to design GWO-PID and GWO-FOPID controllers for the control of DC motor, utilizing an ITAE objective function. Comparative analysis against IWO-PID, PSO-PID, and SFS-PID controllers demonstrated that GWO-PID and GWO-FOPID achieved superior performance with regards to settling time, overshoot, and rise time. In [5], HGSO and OBL/HGSO algorithms were developed to manage the speed of a DC motor using the ITAE objective function. Upon evaluation, the proposed OBL/HGSO algorithm exhibited superior control performance and robustness when compared with ASO, SFS, GWO, and SCA algorithms under both uncertainties and load disturbances.

In a recent development, [41] proposed the Harris Hawk Optimization (HHO) algorithm that leverages a mathematical model which mimic the hunting behavior observed in hawks. The HHO-PID controller was employed to regulate the speed of a DC motor in [38], with the objective of minimizing the ITAE performance criterion. The performance of the proposed control algorithm was evaluated through a comparative study with ASO-PID, GWO-PID, and SCA-PID controllers, utilizing transient response and robustness analyses. Results revealed that the step response of the HHO-PID algorithm demonstrated superior performance, exhibiting lower values for maximum overshoot, rise time, and settling time in comparison to the other controllers. Similarly, the authors in [42] put forward an HHO-based PID/FOPID controller to control the speed of a DC motor. The proposed controller was designed using three objective functions and the result shows better performance when evaluated against established methods like IWO-FOPID/PID, GWO-FOPID/PID, and SFS-FOPID/PID. The study in [43] employed a Non-linear Auto Regressive with eXogenous input (NARX) network

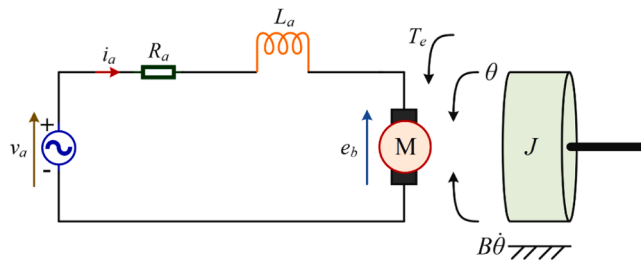


Fig. 1. Equivalent circuit of an externally excited DC motor.

approach to identify system dynamics, utilizing a DC motor and a HHO-tuned FOPID controller as plant and controller, respectively. The proposed technique was evaluated under both step and load response conditions and demonstrated stable and superior performance compared to conventional PID/FOPID controllers.

The majority of meta-heuristics-based PID and FOPID controllers proposed in the literature are susceptible to issues associated with nonlinearity, time-varying dynamics, and significant parameter uncertainties. Such challenges can result in suboptimal control performance, instability, and/or overshoot. To overcome these challenges, in the proposed method, the robustness and adaptability of Harris Hawk Optimization (HHO) algorithm has been explored. This is particularly motivated by the algorithm proficiency in exploring the solution space and identifying optimal parameter values that can compensate for the effects of nonlinearities and uncertainties in the system. Furthermore, this algorithm has significantly shown improvement in the control performance, stability, and robustness in the speed control of DC motor system and others various applications. However, due to the equal perching chance among the Hawks in HHO, with fixed probability of 0.5, the exploration behavior of HHO is limited, random and constrained [20,44].

3.0. System component modeling

The control system under consideration in this study consists of a controller and a plant which in this case is a DC motor. The overall objective of the system is to control the speed and direction of the DC motor. In the following sub-section, we provide a comprehensive description of the mathematical modeling of each of these components.

3.1. Modeling of DC motor

The two commonly used DC motors in industry are the externally and self-excited types. This study focuses on the use of an Externally Excited DC Motor (EEDCM) for speed control of the armature voltage [45]. The EEDCM is composed of two main control sections: the field and armature. Fig. 1 depicts the equivalent electric circuit of the armature along with the free body diagram of the rotor.

The speed control of the DC motor is typically achieved through the manipulation of the armature voltage (V), which generates an electro-

Table 1
DC motor simulation values.

S/N	Variable	Value
1	R_a	0.4 Ω
2	L_a	2.7 H
3	J	0.0004 kg m ²
4	B	0.0022 N m s/rad
5	K_m	0.015 N m/A
6	K_b	0.05 V s

mechanical force when current (i) flows through the circuit in a manner that is proportional to the rotational speed [46]. Applying Kirchhoff Voltage Law and Newton second law of motion to Fig. 1, the differential equation of the armature circuit is as shown in Eq. (1).

$$v_a = i_a R_a + L_a \frac{di_a}{dt} + e_b \quad (1)$$

When the flux remains constant, the induced voltage e_b in the motor is directly proportional to the angular velocity ω as presented in Eq. (2).

$$e_b = K_b \frac{d\theta}{dt} = K_b \omega \quad (2)$$

The torque generated by the armature current is the combined effect of the inertia and frictional torques, resulting in a total torque as depicted in Eq. 3

$$T_e - T_L = J \frac{d\omega}{dt} + B\omega = K_m i_a \quad (3)$$

Where v_a , i_a , R_a and L_a are the applied voltage, current, resistance and inductance of the DC motor armature measured in [V], [A], [Ω] and [H] respectively. e_b and K_b are the back electromotive force and constant measured in [V] and [V.s/rad] respectively. Also, θ and ω are the angular speed and velocity of the motor shaft in [rad/s]. T_e , T_L and J are the electric torque, load torque and moment of inertia of the motor in [N.m] and kg m² respectively. B and K_m are frictional and torque constants of the motor in N.m.s/rad and N.m/A respectively.

Applying Laplace transform and setting initial conditions to zero to Eqs. (1–3), yields equations (4–6):

$$V_a(s) = (L_a s + R_a) I_a(s) + E_b(s) \quad (4)$$

$$E_b(s) = K_b \omega(s) \quad (5)$$

$$T_e(s) - T_L(s) = (J s + B) \omega(s) = K_m I_a(s) \quad (6)$$

Substituting Eq. (5) in 4 and simplifying Eq. (4) and 6 yields Eq. (7) and 8:

$$I_a(s) = \frac{V_a(s) - K_b \omega(s)}{(L_a s + R_a)} \quad (7)$$

$$\omega(s) = \frac{T_e(s) - T_L(s)}{(J s + B)} = \frac{K_m}{(J s + B)} I_a(s) \quad (8)$$

The block diagram of a separately excited DC Motor is as shown in

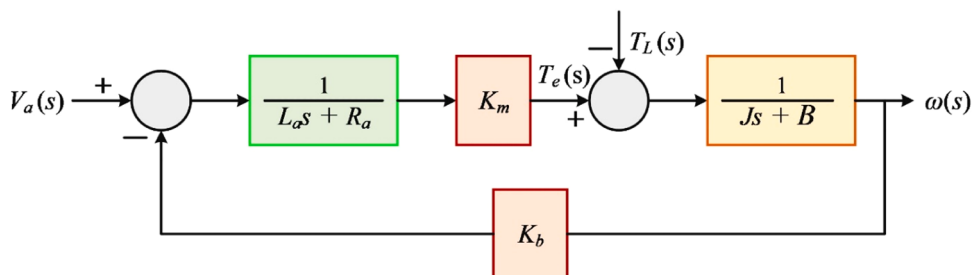


Fig. 2. Block diagram illustrating the structure of a separately excited DC Motor.

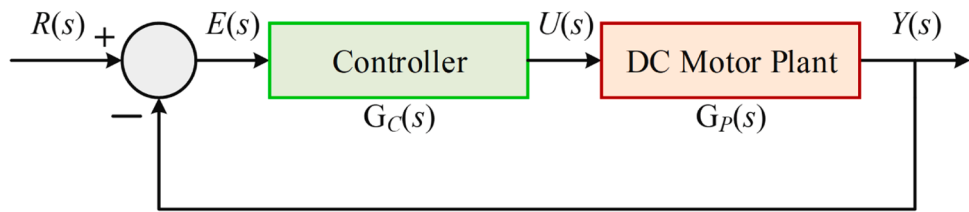


Fig. 3. Block Diagram of a DC motor with controller.

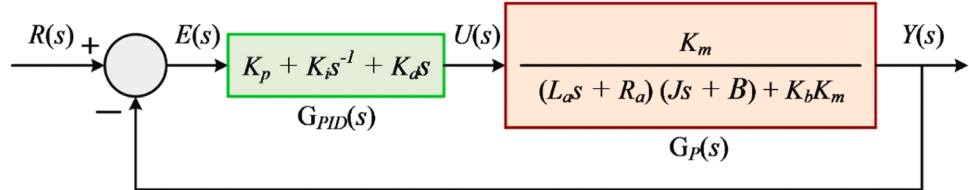


Fig. 4. Block Diagram of a PID-controller DC motor.

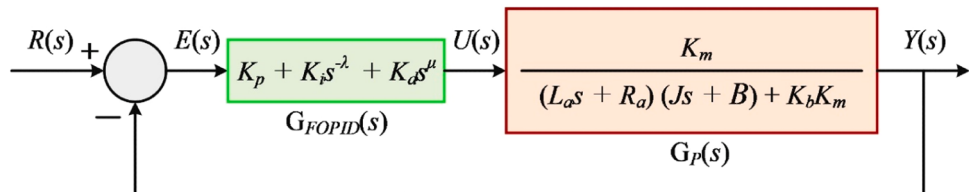


Fig. 5. Block diagram of a FOPID-controlled DC motor.

Table 2
List of commonly used objective functions.

S/ N	Objective Function	Expression	Equation number
1	Integral of Absolute Error (IAE)	$IAE = \int_0^{t_{\text{sim}}} e(t) dt$	20
2	Integral Squared Error (ISE)	$ISE = \int_0^{t_{\text{sim}}} e^2(t) dt$	21
3	Integral of Time multiplied Absolute Error (ITAE)	$ITAE = \int_0^{t_{\text{sim}}} t e(t) dt$	22
4	Integral of Time multiplied Squared Error (ITSE)	$ITSE = \int_0^{t_{\text{sim}}} t e^2(t) dt$	23
5	Integral of Squared Time multiplied by Square Error (ISTSE)	$ISTSE = \int_0^{t_{\text{sim}}} t^2 e^2(t) dt$	24
6	Integral of Squared Time multiplied by Error, all to be squared (ISTES)	$ISTES = \int_0^{t_{\text{sim}}} t^2 e(t) ^2 dt$	25

Fig. 2. The transfer function representing the relationship between from input voltage $V_a(s)$ and output motor speed $\omega(s)$ of the DC motor, in the absence of load torque can be expressed by Eq. (9).

$$G_p(s) = \frac{\omega(s)}{V_a(s)} = \frac{K_m}{(L_a s + R_a)(J s + B) + K_b K_m} \quad \text{for } T_L(s) = 0 \quad (9)$$

For simulation, the parameter values outlined in Table 1 were employed, as referenced in previous studies [4,42,47–50]. By substituting these values into Eq. (9), we obtain Eq. (10). Furthermore, through the simplification process, Eq. (11) is derived.

$$G_p(s) = \frac{0.015}{(2.7s + 0.4)(0.0004s + 0.0022) + 0.00075} \quad (10)$$

$$G_p(s) = \frac{15}{1.08s^2 + 6.1s + 1.63} \quad (11)$$

3.2. DC motor speed control with controllers

In control engineering, controller systems serve as a means of connecting the process variable, which denotes the current state of a system, with the setpoint, reflecting the desired state of the system. These systems are utilized to increase the accuracy of continuous states by reducing steady state error and improving the response time of an over-damped system [51]. The two commonly employed controllers for regulating the speed of a DC motor are PID and FOPID. Fig. 3 depicts the block diagram of a general DC motor speed controller.

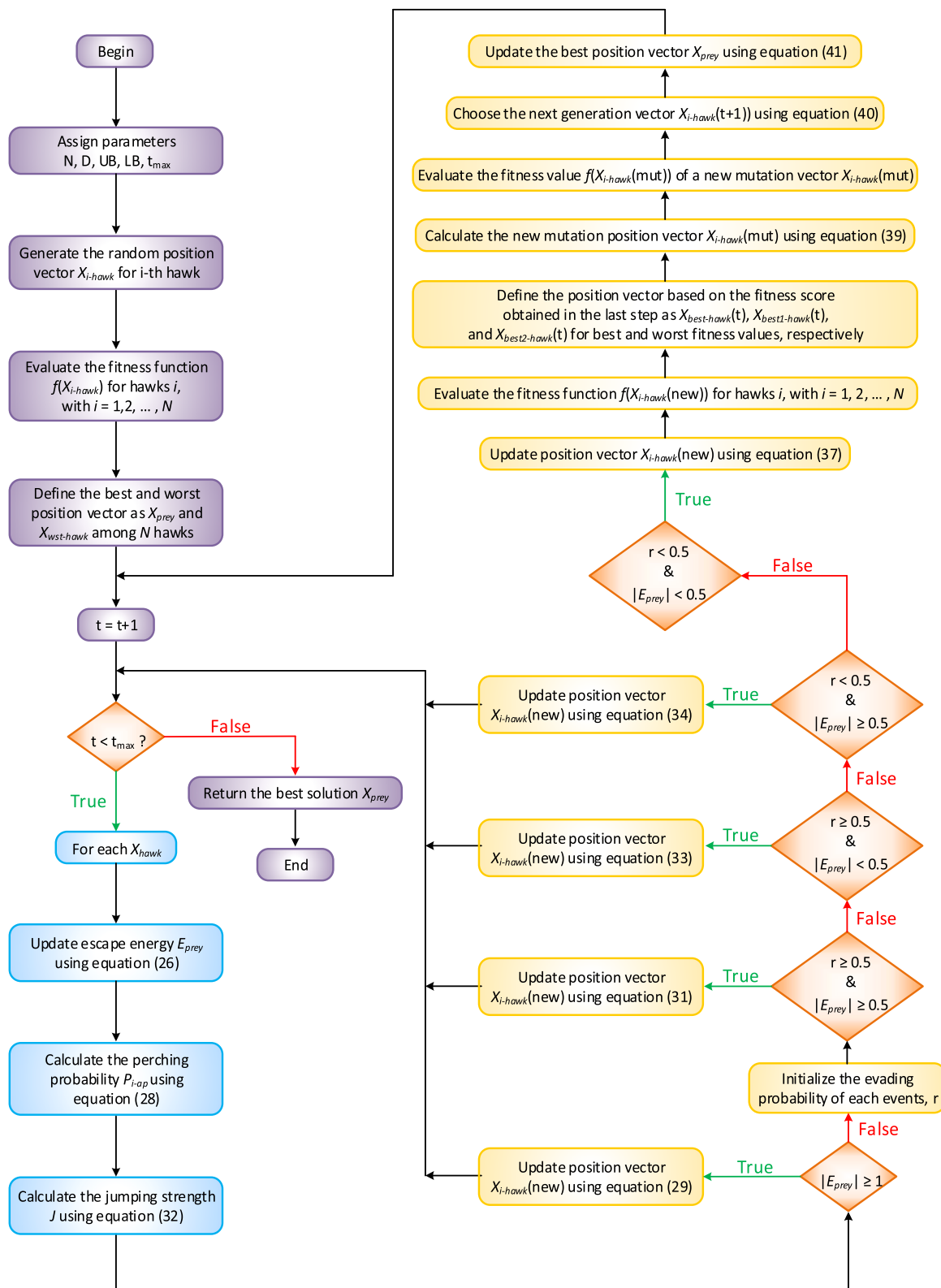
3.2.1. DC motor speed control with PID controller

In process control industries, PID controllers are widely adopted due to their numerous advantages. The stability analysis of these controllers is notably simple, and they can be easily tuned. PID control utilizes a closed loop control feedback mechanism to maintain the actual output as closely as possible to the setpoint. The time-domain representation and transfer function of a PID controller are given as shown in Eqs. (12) and (13).

$$u(t) = K_p e(t) + K_i \int e(t) + K_d \frac{d}{dt} e(t) \quad (12)$$

$$G_{PID}(s) = K_p + \frac{K_i}{s} + K_d s = \frac{K_p s + K_i + K_d s^2}{s} = K_p + K_i s^{-1} + K_d s \quad (13)$$

From Fig. 4, the closed-loop transfer function of the PID-controlled DC Motor with unity feedback is given as presented by Eq. (14).

**Fig. 6.** Flowchart of the LHHO algorithm for speed control of DC motor.

Algorithm 1

Pseudo-code of LHHO algorithm.

Algorithm 1: Pseudo-code of LHHO algorithm	
1	/* initialization */
2	Set algorithm parameters N, D, t_{max} , UB, LB;
3	Generate random position vector X_{i-hawk} for i^{th} hawk at $t = 1$
4	Begin
5	Evaluate the fitness function $f(X_{i-hawk})$ for hawks i with $i = 1, 2, \dots, N$
6	Define the best and worst position vector as X_{prey} and $X_{wst-hawk}$ among N hawks from 1
7	while $t < t_{max}$ do
8	foreach hawk i in population do
9	Update the escaping energy (E_{prey}) using Eq. 26
10	Calculate adaptive perching probability (P_{i-ap}) using Eq. 28
11	Calcualte the jumping strength (N) using Eq. 32
12	/*exploration stage*/
13	if escaping energy $ E_{prey} \geq 1$ do
14	Update the new position vector $X_{i-hawk}(new)$ using Eq. 29
15	else
16	/*exploitation stage*/
17	if $ E_{prey} < 1$ do
18	initialize the evading probability of each events, r
19	/*soft besiege*/
20	if ($r \geq 0.5$ and $ E_{prey} \geq 0.5$) do
21	Update the position vector $X_{i-hawk}(new)$ using Eq. 31
22	else
23	/*hard besiege*/
24	if ($r \geq 0.5$ and $ E_{prey} < 0.5$) do
25	Update the position vector $X_{i-hawk}(new)$ using Eq. 33
26	else
27	/* soft besiege with rapid dive */
28	if ($r < 0.5$ and $ E_{prey} \geq 0.5$) do
29	Update the position vector $X_{i-hawk}(new)$ using Eq. 34
30	else
31	/* hard besiege with rapid dive */
32	if ($r < 0.5$ and $ E_{prey} < 0.5$) do
33	Update the position vector $X_{i-hawk}(new)$ using Eq. 37
34	end
35	end
36	Evaluate the fitness function $f(X_{i-hawk})$ for hawks i with $i = 1, 2, \dots, N$
37	Define the best three fitness from (ii) as $X_{best-hawk}(t)$, $X_{best1-hawk}(t)$ and $X_{best2-hawk}(t)$
38	end
39	for $X_{i-hawk}(new)$ do
40	Calculate the new mutation position vector $X_{i-hawk}(mut)$ using Eq. 39
41	Evaluate the fitness value $f(X_{i-hawk}(mut))$ of a new mutation vector $X_{i-hawk}(mut)$
42	Choose the next generation vector $X_{i-hawk}(t + 1)$ using Eq. 40
43	Update the best position vector as X_{prey} using Eq. 41
44	end
45	Set $t = t + 1$
46	return the best solution X_{prey}
47	end
48	end

$$G_{DC_PID}(s) = \frac{G_{PID}(s) \times G_{DC}(s)}{1 + G_{PID}(s) \times G_{DC}(s)} \quad (14)$$

When we substitute $G_{PID}(s)$ and $G_{DC}(s)$ in Eqs. (13) and 9 into 14, we have Eq. (15)

$$G_{DC_PID}(s) = \frac{K_m(K_p + K_i s^{-1} + K_d s)}{[(Js + B)(L_a s + R_a) + K_b K_m + K_m(K_p + K_i s^{-1} + K_d s)]} \quad (15)$$

3.2.2. DC motor speed control with FOPID controller

Fractional order PID (FOPID) controllers possess two additional tuning parameters (λ, μ) compared to integer order PID controllers. These controllers are known for their ability to remain stable despite changes in the parameters of the controlled system and the controller itself [19]. The time-domain representation and transfer function of a FOPID controller are as given in Eqs. (16) and 17 respectively.

$$u(t) = K_p e(t) + K_i D_t^{-\lambda} e(t) + K_d D_t^{\mu} e(t) \quad (16)$$

Table 3

Parameters of LHHO-PID/FOPID algorithm.

Parameter	Value
Number of Hawks (Population size) (N)	100
Levy flight constant (β)	1.5
Number of iterations (t_{max})	50
PID/FOPID controller dimension (D)	3/5
Lower bounds ($K_p, K_i, K_d, \lambda, \mu$)	[0.001 0.001 0.001 0 0]
Upper bounds ($K_p, K_i, K_d, \lambda, \mu$)	[20 20 20 1 1]
Simulation time (t_{sim})	0.5 s

$$G_{FOPID}(s) = K_p + K_i s^{-\lambda} + K_d s^{\mu} \quad (17)$$

where $u(t)$ is the desired signal, $e(t)$ is the error signal, $D_t^{-\lambda}$ and D_t^{μ} are the integral and differential operators of the fractional order.

Similarly, from Fig. 5, the closed-loop transfer function of the FOPID-controlled DC Motor with unity feedback is given by Eq. (18).

$$G_{DC_FOPID}(s) = \frac{G_{FOPID}(s) \times G_{DC}(s)}{1 + G_{FOPID}(s) \times G_{DC}(s)} \quad (18)$$

When we substitute $G_{FOPID}(s)$ and $G_{DC}(s)$ in Eqs. (17) and 9 into 18, we have Eq. (19).

$$G_{DC_FOPID}(s) = \frac{K_m(K_p + K_i s^{-\lambda} + K_d s^{\mu})}{[(Js + B)(L_a s + R_a) + K_b K_m + K_m(K_p + K_i s^{-\lambda} + K_d s^{\mu})]} \quad (19)$$

3.2. Objective functions

The objective function is a fundamental performance criterion used during optimization of PID and FOPID controllers design parameters to achieve specific control objectives. These objectives may include but not limited to reducing the overshoot, settling time, steady-state error, and attaining stability. Its primary purpose is to minimize the difference between the desired and actual system outputs, which serves as a measure of the controller's performance. Numerous objective functions have been utilized in the previous studies to achieve precise speed regulation of DC motors to a pre-defined setpoint. Table 2 present the widely adopted objective functions for DC motor speed regulation where $e(t)$ is the error signal which is the disparity between reference input and actual speed and t_{sim} is the simulation time.

4.0. LHHO algorithm

Design parameter tuning of PID and FOPID controllers often presents a significant challenge and involves the use of fractional integral-

Table 4

Lowest achievable loss values from the objective functions.

S/ N	Algorithm-Controller	Objective Function			
		IAE	ISE	ITSE	
1	LHHO-PID (Proposed)	0.018477	0.006578	0.000063	0.000401
2	HHO-PID [38]	0.091917	0.164402	0.00321	0.003993
3	ASO-PID [35]	0.092574	0.164867	0.003262	0.003422
4	PSO-PID [6]	0.114495	0.165158	0.003729	0.003265
5	IGWO-PID [34]	0.11447	0.165108	0.0037	0.003214
6	LHHO-FOPID (Proposed)	0.008502	0.003000	1.35E-05	0.000132
7	HHO-FOPID [42]	0.042901	0.074981	0.001096	0.001346
8	ASO-FOPID [4]	0.048411	0.077073	0.00138	0.002861
9	PSO-FOPID [6]	0.068159	0.076024	0.001553	0.014806
10	IGWO-FOPID [34]	0.068215	0.076024	0.001553	0.014853

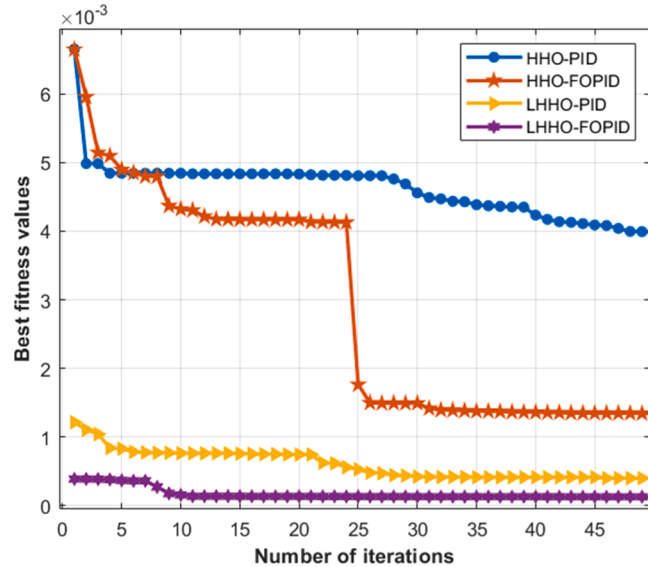


Fig. 8. ITAE-based Convergence curve for the proposed controllers and the baseline.

differential equations [52]. One of the existing methods for parameter tuning in PID and FOPID involves the use of meta-heuristics optimization algorithms. Over the years, several meta-heuristics algorithms such as PSO [6], ASO [35], IGWO [34], etc. have been successfully applied to optimal tuning of PID and FOPID controllers. However, to the best of our knowledge, existing study that explored the adaptive perching probability and leadership prowess in Leader Harris Hawks Optimizer (LHHO)

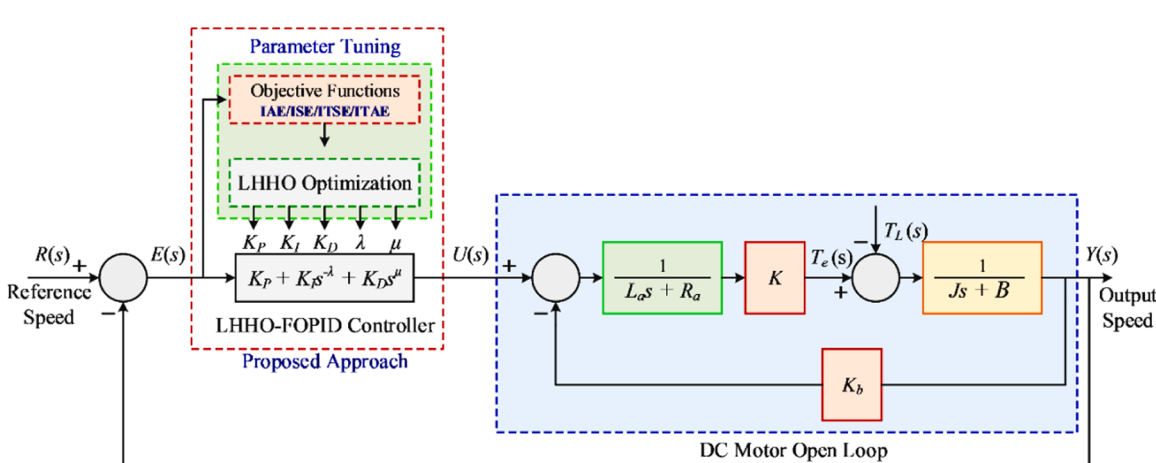


Fig. 7. Block diagram of the proposed DC Motor with LHHO-FOPID Controller.

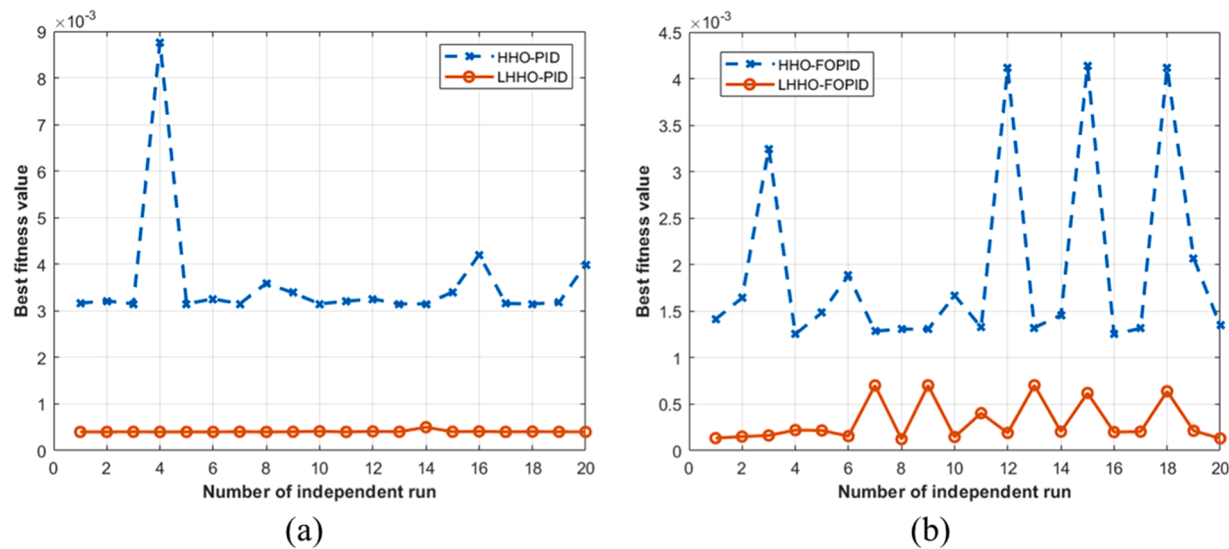


Fig. 9. Plot of ITAE-based best fitness score obtained from all independent runs of HHO and LHHO algorithm for (a) PID gain parameter tuning (b) FOPID gain parameter tuning.

Table 5
Statistical values of ITAE objective function for the proposed controller and its baseline.

S/N	Algorithm-Controller	Statistical index				
		Best	Worst	Mean	Median	Standard deviation
1	LHHO-PID (Proposed)	0.0004004	0.0005018	0.0004087	0.0004032	0.00002225
2	HHO-PID	0.0032	0.0088	0.0036	0.0032	0.0013
3	LHHO-FOPID (Proposed)	0.0001237	0.0007040	0.0003118	0.0002046	0.000223
4	HHO-FOPID	0.0004004	0.0005018	0.0004087	0.0004032	0.00002225

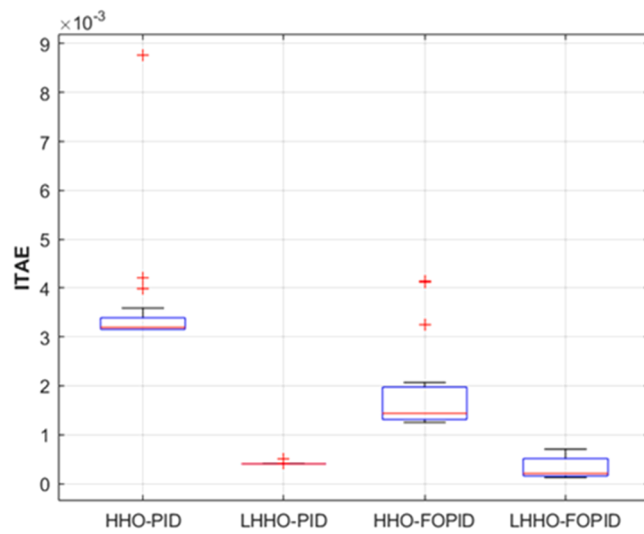


Fig. 10. Boxplot of ITAE-based best fitness score obtained from all independent runs of HHO and LHHO for PID and FOPID controllers.

for DC motor speed control has been limited. The Harris hawk's optimization technique is a population-based, meta-heuristic algorithm that takes inspiration from the hunting and cooperating pattern of the hawks. This approach was first introduced by [41]. A group of hawks collaboratively targets their prey, primarily rabbits, launching coordinated attacks from various angles and converging on the unsuspecting target [44]. Each hawk in a group possesses a distinct solution to an optimization problem, all with an equal likelihood. The most optimal solution among them is then considered as the precise location of the rabbit.

There are two distinct and structured phases within the algorithm referred to as exploitation and exploration. At the exploration stage, the algorithm conducts a global search for optimal solutions, while in the exploitation phase, it focuses on a local search.

Despite having a higher computational complexity, the Harris hawk's optimization method exhibits a better convergence rate than other comparable algorithms [20]. The exploration behavior of the Harris hawk's optimization (HHO) algorithm is, however, limited by its equal perching likelihood among the hawks, with a fixed probability of 0.5. As a result, its exploration is random and constrained. To overcome this limitation, Naik et al. [44] suggested the utilization of an adaptive perch probability. This probability is determined based on the fitness levels of the Harris hawks during an exploration phase. The Leader Harris Hawks Optimization (LHHO) technique is employed to improve the searching potential of the HHO algorithm. LHHO increases exploration by using an adaptive perching approach during the exploration stage and a leader-based mutation-selection mechanism through every generation of Harris Hawks. Fig. 6 provides a flowchart with comprehensive step-by-step details of the proposed algorithm. Furthermore, pseudo-code of the algorithm is also presented in Algorithm 1.

The shift from exploration to exploitation is dependent upon the prey's escaping energy, E , confined within a specific range. The position vector of the hawk and current position of the prey are respectively denoted by X_{hawk} and X_{prey} . Thus, the escaping energy of the prey, E_{prey} can be modelled as function of maximum number of iterations t_{max} , current iteration t and initial energy of the prey E_{o-prey} as shown in Eq. (26).

$$E_{prey} = 2E_{o-prey} \left[1 - \frac{t}{t_{max}} \right] \quad (26)$$

Where E_{o-prey} randomly takes values in the range of (-1,1) at each iteration and can be estimated as given in Eq. (27).

Table 6

Gains of the proposed LHHO-PID/FOPID controllers and other compared approaches.

S/N	Algorithm-Controller	Gain parameters				λ	μ
		K_p	K_i	K_d			
1	LHHO-PID (Proposed)	19.99999	5.437263	3.359391	—	—	—
2	HHO-PID [38]	19.9994	5.4036	3.3582	—	—	—
3	ASO-PID [35]	18.74551157	12.33363059	13.83286123	—	—	—
4	PSO-PID [6]	19.6586	4.8951	3.2216	—	—	—
5	IGWO-PID [34]	19.66287869	5.427335562	3.184861028	—	—	—
6	LHHO-FOPID (Proposed)	19.92098344	19.9135272	6.413580242	0.136910984	0.995520089	—
7	HHO-FOPID [42]	4.4197	19.6228	5.8509	0.1146	0.9717	—
8	ASO-FOPID [4]	14.15164029	17.59827293	13.22960153	0.369001134	0.736997576	—
9	PSO-FOPID [6]	20	19.4923	20	0.749	0.5816	—
10	IGWO-FOPID [34]	19.948	19.9271	19.9921	0.735	0.5914	—

Table 7

Step response of the proposed and various other approaches.

S/N	Algorithm-Controller	Rise time (t_r) (s)	Settling time (t_s) (s)	Maximum overshoot (M_p) (%)	Steady State Error (E_{ss})
1	LHHO-PID (Proposed)	0.0463	0.0794	0.2657	5.6374e-04
2	HHO-PID [38]	0.0463	0.0795	0.2664	5.3602e-04
3	ASO-PID [35]	0.0123	0.0835	0	0.0110
4	PSO-PID [6]	0.0478	0.0809	0.4203	3.5644e-04
5	IGWO-PID [34]	0.0482	0.0808	0.5326	9.5651e-04
6	LHHO-FOPID (Proposed)	0.0254	0.0453	0.0456	7.8875e-04
7	HHO-FOPID [42]	0.0318	0.0641	0	0.0055
8	ASO-FOPID [4]	0.0265	0.1258	8.0645	0.0064
9	PSO-FOPID [6]	0.0265	0.1267	17.5882	0.0046
10	IGWO-FOPID [34]	0.0260	0.1257	16.7203	0.0046

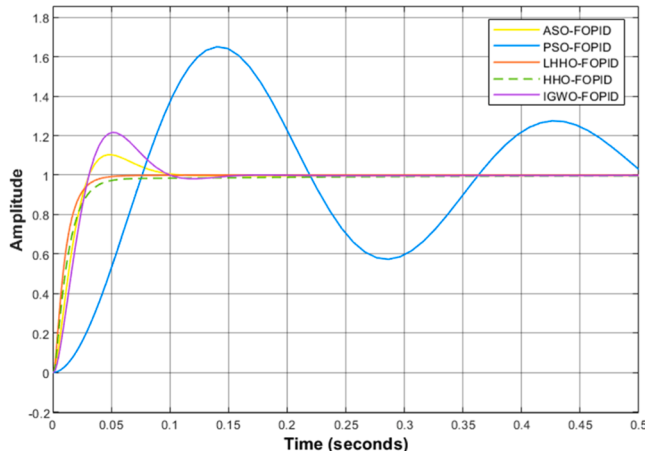


Fig. 11. Step response of the proposed LHHO-FOPID with existing FOPID controllers.

$$E_{o-prey} = 2 * \text{rand}(.) - 1 \quad (27)$$

When the value of E_{o-prey} decreases from 0 to -1 , it signifies a decline in the physical strength of the prey. Conversely, an increase in the value of E_{o-prey} from 0 to 1, means that the rabbit is strengthening. The dynamic escaping energy E_{prey} demonstrates a decreasing trend throughout the iterations. When the escaping energy $|E_{prey}| \geq 1$, the hawks initiate a search operation in various regions to locate the rabbit. On the other hand, when $|E_{prey}| < 1$, the hawks attempt to exploit the nearby solutions. Moreover, exploration happens when $|E_{prey}| \geq 1$, while exploitation occurs when $|E_{prey}| < 1$.

4.1. Exploration phase ($|E_{prey}| \geq 1$)

The hawk initiates a perching strategy and remains stationary scanning the surroundings for potential prey at a random location. The adaptive perching probability (P_{i-ap}) of i^{th} hawk is employed to choose

the best perching strategy as given in Eq. (28). It is normally a function of the current i^{th} hawk value with position vector (X_{i-hawk}), position of the worst-performing hawk ($X_{wst-hawk}$), and vector position of the prey (X_{prey}).

$$P_{i-ap} = \frac{|f(X_{i-hawk}) - f(X_{prey})|}{|f(X_{wst-hawk}) - f(X_{prey})|} \quad (28)$$

For $i = 1, 2, 3\dots$

The updated position of the hawk can be modelled as given in Eq (29).

$$X_{i-hawk}(new) = \begin{cases} (X_{rand-hawk}(t) - r_1)(X_{rand-hawk}(t) - 2r_2X_{i-hawk}(t)) & q \geq P_{i-ap} \\ (X_{prey}(t) - (X_{m-hawk}(t))) - r_3(LB + r_4(UB - LB)) & q < P_{i-ap} \end{cases} \quad (29)$$

Where $X_{rand-hawk}(t)$ denotes the position vector of a randomly selected hawk during iteration t . LB and UB are the lower and upper bound of the search space whereas r_1, r_2, r_3, r_4, q are set of random numbers in the

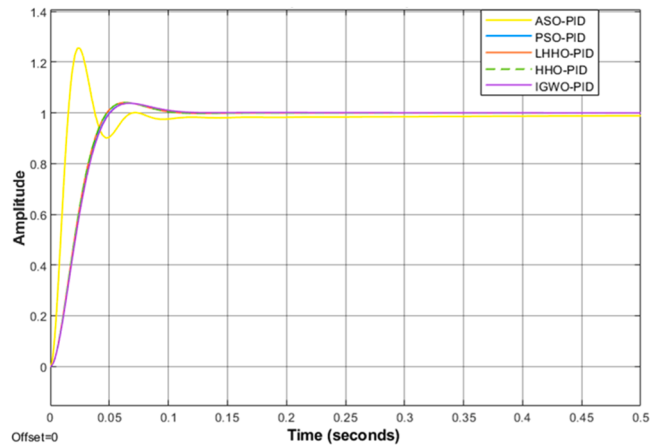


Fig. 12. Step response of the proposed LHHO-PID with existing PID-controllers.

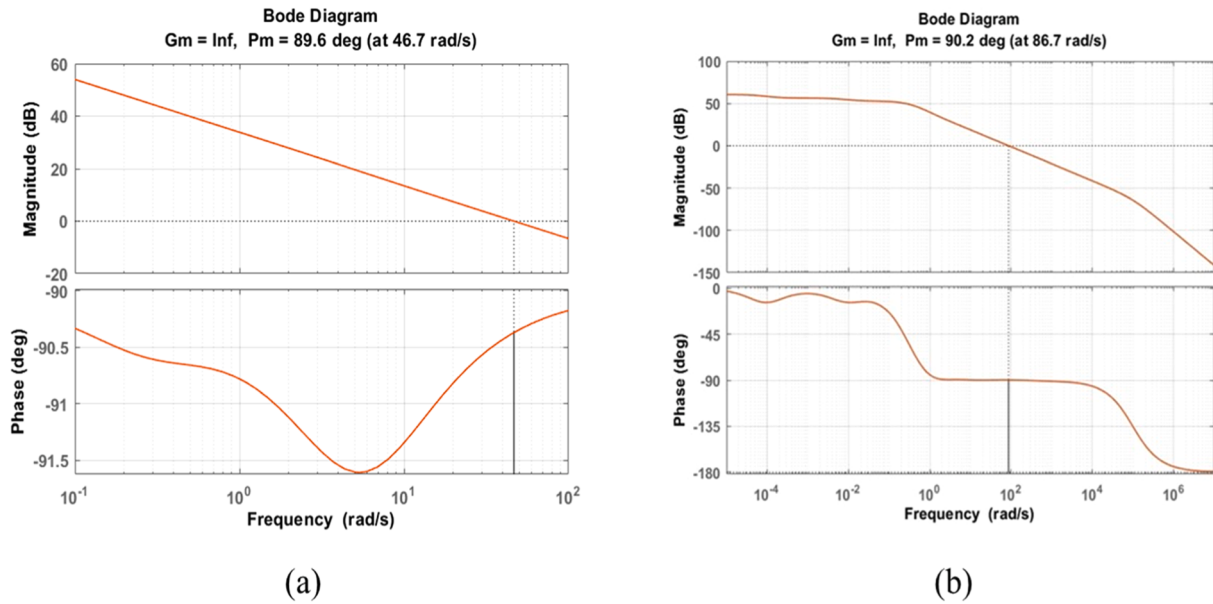


Fig. 13. Bode plot of DC motor speed control with (a) LHHO-PID controller (b) LHHO-FOPID controller.

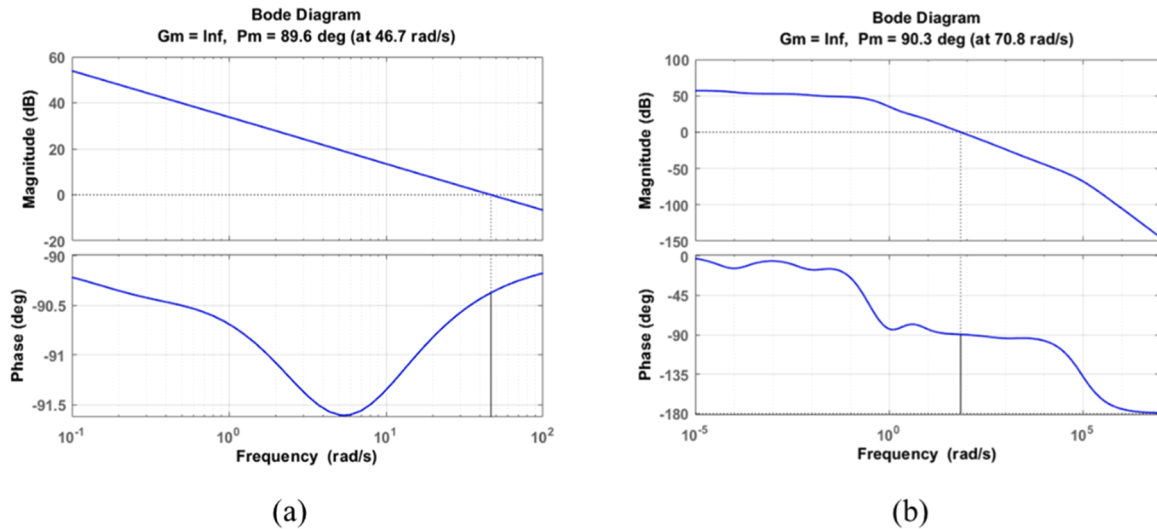


Fig. 14. Bode plot of DC motor speed control with (a) HHO-PID controller (b) HHO-FOPID controller.

range (0, 1). The mean position of all the N Hawks in the generation t is represented as $X_{m-hawk}(t)$, and can be computed for N number of Hawk using Eq. (30).

$$X_{m-hawk}(t) = \frac{1}{N} \sum_1^N X_{i-hawk}(t) \quad (30)$$

4.2. Exploitation phase ($|E_{prey}| < 1$)

During this phase, the Hawks executes various attacking strategies on the identified prey, and the nature of these strategies will be determined by the escaping patterns and energy levels of the rabbit. The Hawks will strategically position themselves around the prey, implementing a set of the following four distinct strategies to encircle it effectively [44].

4.2.1. Soft besiege ($r \geq 0.5$ and $|E_{prey}| \geq 0.5$)

This strategy is followed when both the evading probability of the Hawk and its escaping energy is more than 50 %. The new position

vector of the i^{th} hawks is governed by Eq. (31).

$$X_{i-hawk}(new) = X_{prey}(t) - X_{i-hawk}(t) - E_{prey} |JX_{prey}(t) - X_{i-hawk}(t)| \quad (31)$$

where J is the jumping strength of the prey throughout the escaping attempt randomly changes (between 0 and 1) to simulate the nature of the prey motions as given in Eq. (32).

$$J = 2(1 - r_5) \quad (32)$$

4.2.2. Hard besiege ($r \geq 0.5$ and $|E_{prey}| < 0.5$)

Here, the probability of prey evading the Hawk hunt is more than 50 % but its escaping energy E_{prey} is less than 50 %. The new position vector of the i^{th} hawks is given in Eq. (33).

$$X_{i-hawk}(new) = X_{prey}(t) - E_{prey} |X_{prey}(t) - X_{i-hawk}(t)| \quad (33)$$

4.2.3. Soft besiege with progressive rapid dives ($r < 0.5$ and $|E_{prey}| \geq 0.5$)

Here, the escaping energy E_{prey} is greater than 0.5, but the probability of prey evading the Hawk hunt is less than 50 %. The incorporation of

Table 8

Frequency analysis result of the speed control system with different controllers.

S/N	Algorithm-Controller	Gain margin (dB)	Phase margin (°)	Phase crossover frequency (rad/s)	Bandwidth (Hz)
1	LHHO-PID (Proposed)	Infinite	89.6305	46.6933	46.8832
2	HHO-PID [38]	Infinite	89.6280	46.6772	46.8690
3	ASO-PID [35]	Infinite	91.2804	192.0480	187.2379
4	PSO-PID [6]	Infinite	89.4288	44.8028	45.1413
5	IGWO-PID [34]	Infinite	89.3307	44.2988	44.7085
6	LHHO-FOPID (Proposed)	Infinite	90.2218	86.7057	86.3234
7	HHO-FOPID [42]	Infinite	90.3028	70.8014	70.4507
8	ASO-FOPID [4]	Infinite	74.6657	57.3245	71.6130
9	PSO-FOPID [6]	Infinite	60.0179	48.2264	68.4871
10	IGWO-FOPID [34]	Infinite	61.2981	49.5646	69.9076

Table 9

Operating scenarios with different DC motor parameters.

Parameter	Scenarios							
	I	II	III	IV	V	VI	VII	VIII
R_a	0.3	0.3	0.5	0.5	0.2	0.2	0.6	0.6
K_m	0.012	0.018	0.012	0.018	0.009	0.021	0.009	0.021

Table 10Step response result for scenario 1 when $R_a = 0.3$ and $K_m = 0.012$.

S/N	Algorithm-Controller	Rise time (t_r) (s)	Settling time (t_s) (s)	Max. overshoot (M_p) (%)	Steady State Error (E_{SS})
1	LHHO-PID (Proposed)	0.0575	0.0974	0.4264	0.0022
2	HHO-PID [38]	0.0575	0.0974	0.4265	0.0021
3	ASO-PID [35]	0.0157	0.0330	0	0.0130
4	PSO-PID [6]	0.0593	0.0988	0.5835	0.0020
5	IGWO-PID [34]	0.0603	0.1013	0.4398	0.0027
6	LHHO-FOPID (Proposed)	0.0317	0.0562	0.0754	1.7058e-04
7	HHO-FOPID [42]	0.0401	0.0848	0	0.0058
8	ASO-FOPID [4]	0.0320	0.1410	8.6088	0.0072
9	PSO-FOPID [6]	0.0313	0.2253	18.5011	0.0052
10	IGWO-FOPID [34]	0.0308	0.2184	17.6335	0.0052

Table 11Frequency analysis result of the system for scenario 1 when $R_a = 0.3$ and $K_m = 0.012$.

S/N	Algorithm-Controller	Gain margin (dB)	Phase margin (°)	Phase crossover frequency (rad/s)	Bandwidth (Hz)
1	LHHO-PID (Proposed)	Infinite	89.4841	37.3666	37.6133
2	HHO-PID [38]	Infinite	89.4810	37.3539	37.6025
3	ASO-PID [35]	Infinite	91.5870	153.5742	148.9093
4	PSO-PID [6]	Infinite	89.2327	35.8642	36.2561
5	IGWO-PID [34]	Infinite	89.1103	35.4637	35.9257
6	LHHO-FOPID (Proposed)	Infinite	90.2103	69.2560	68.9610
7	HHO-FOPID [42]	Infinite	90.4766	56.6066	56.1482
8	ASO-FOPID [4]	Infinite	73.2479	47.0333	59.1325
9	PSO-FOPID [6]	Infinite	58.0602	40.7684	57.8989
10	IGWO-FOPID [34]	Infinite	59.3584	41.7763	58.9480

the levy flight function (LF) introduces an enhanced fleeing model for the prey, resulting in more realistic and effective movement patterns. The Hawk utilizes distinct approaches, depicted in Eqs. (34–36), to determine its optimal move based on the current circumstances and objectives.

$$X_{i-hawk}(new) = \begin{cases} Y_{i-hawk} & \text{if } f(Y_{i-hawk}) \langle f(X_{i-hawk}(t)) \\ Z_{i-hawk} & \text{if } f(Z_{i-hawk}) \langle f(X_{i-hawk}(t)) \end{cases} \quad (34)$$

$$Y_{i-hawk} = X_{prey}(t) - E_{prey} |JX_{prey}(t) - X_{i-hawk}(t)| \quad (35)$$

$$Z_{i-hawk} = Y_{i-hawk} + S \times LF(D) \quad (36)$$

Where the vector S represent a random element of dimension $1 \times D$, D corresponds to the dimensionality of the problem at hand and LF denotes the levy flight movements as defined in [53].

4.2.4. Hard besiege with progressive rapid dives ($r < 0.5$ and $|E_{prey}| < 0.5$)

Here, the escaping energy E_{prey} and the probability of prey evading the Hawk hunt are assumed to be less than 50 %. So, the update hawk position is given in Eqs. (37) and 38.

$$X_{i-hawk}(new) = \begin{cases} Y_{i-hawk} & \text{if } f(Y_{i-hawk}) \langle f(X_{i-hawk}(t)) \\ Z_{i-hawk} & \text{if } f(Z_{i-hawk}) \langle f(X_{i-hawk}(t)) \end{cases} \quad (37)$$

$$Y_{i-hawk} = X_{prey}(t) - E_{prey} |JX_{prey}(t) - X_{m-hawk}(t)| \quad (38)$$

1.9. Leader-based mutation selection

The exploration of the process is further expanded by implementing an additional phase that involves a mutation selection approach. This is done to reduce the chances of local optimal by defining the best Hawk position $X_{best-hawk}(t)$, the second-best position $X_{best1-hawk}(t)$ and the third-best position $X_{best2-hawk}(t)$ using the value of the fitness function of

Table 12Step response result for scenario 2 when $R_a = 0.3$ and $K_m = 0.018$.

S/ N	Algorithm- Controller	Rise time (t_r) (s)	Settling time (t_s) (s)	Max. overshoot (M_p) (%)	Steady State Error (E_{SS})
1	LHHO-PID (Proposed)	0.0386	0.0663	0.2815	6.4430e-04
2	HHO-PID [38]	0.0386	0.0663	0.2824	6.2123e-04
3	ASO-PID [35]	0.0101	0.0259	0	0.0090
4	PSO-PID [6]	0.0399	0.0676	0.4322	4.6598e-04
5	IGWO-PID [34]	0.0403	0.0677	0.5322	9.5827e-04
6	LHHO-FOPID (Proposed)	0.0211	0.0377	0	5.4397e-04
7	HHO-FOPID [42]	0.0263	0.0513	0	0.0043
8	ASO-FOPID [4]	0.0227	0.1150	7.6314	0.0052
9	PSO-FOPID [6]	0.0229	0.1157	16.8547	0.0037
10	IGWO-FOPID [34]	0.0224	0.1149	15.9911	0.0037

Table 13Frequency analysis result of the system for scenario 2 when $R_a = 0.3$ and $K_m = 0.018$.

S/ N	Algorithm- Controller	Gain margin (dB)	Phase margin (°)	Phase crossover frequency (rad/s)	Bandwidth (Hz)
1	LHHO-PID (Proposed)	Infinite	89.6531	56.0218	56.2277
2	HHO-PID [38]	Infinite	89.6510	56.0023	56.2101
3	ASO-PID [35]	Infinite	91.0578	230.4648	225.6313
4	PSO-PID [6]	Infinite	89.4823	53.7449	54.1014
5	IGWO-PID [34]	Infinite	89.3997	53.1379	53.5662
6	LHHO-FOPID (Proposed)	Infinite	90.1623	104.1724	103.7819
7	HHO-FOPID [42]	Infinite	90.0903	85.0209	84.8713
8	ASO-FOPID [4]	Infinite	75.4721	67.7209	84.4362
9	PSO-FOPID [6]	Infinite	61.4415	55.6401	79.1860
10	IGWO-FOPID [34]	Infinite	62.6795	57.3413	81.0120

Table 14Step response result for scenario 3 when $R_a = 0.5$ and $K_m = 0.012$.

S/ N	Algorithm- Controller	Rise time (t_r) (s)	Settling time (t_s) (s)	Max. overshoot (M_p) (%)	Steady State Error (E_{SS})
1	LHHO-PID (Proposed)	0.0578	0.0992	0.2373	4.5255e-04
2	HHO-PID [38]	0.0578	0.0992	0.2374	4.1804e-04
3	ASO-PID [35]	0.0157	0.0322	0	0.0141
4	PSO-PID [6]	0.0596	0.1006	0.3892	2.1214e-04
5	IGWO-PID [34]	0.0600	0.1002	0.5174	9.7751e-04
6	LHHO-FOPID (Proposed)	0.0318	0.0566	0.0012	0.0012
7	HHO-FOPID [42]	0.0402	0.0869	0	0.0074
8	ASO-FOPID [4]	0.0321	0.1401	8.4822	0.0082
9	PSO-FOPID [6]	0.0314	0.2272	18.3473	0.0059
10	IGWO-FOPID [34]	0.0309	0.2207	17.4854	0.0059

Table 15Frequency analysis result of the system for scenario 3 when $R_a = 0.5$ and $K_m = 0.012$.

S/ N	Algorithm- Controller	Gain margin (dB)	Phase margin (°)	Phase crossover frequency (rad/s)	Bandwidth (Hz)
1	LHHO-PID (Proposed)	Infinite	89.5977	37.3663	37.5394
2	HHO-PID [38]	Infinite	89.5947	37.3536	37.5286
3	ASO-PID [35]	Infinite	91.6143	153.6037	148.8327
4	PSO-PID [6]	Infinite	89.3511	35.8639	36.1827
5	IGWO-PID [34]	Infinite	89.2301	89.2301	35.8524
6	LHHO-FOPID (Proposed)	Infinite	90.2716	69.2557	68.9302
7	HHO-FOPID [42]	Infinite	90.5516	56.6064	56.1269
8	ASO-FOPID [4]	Infinite	73.3364	47.0231	59.0765
9	PSO-FOPID [6]	Infinite	58.1608	40.7559	57.8553
10	IGWO-FOPID [34]	Infinite	59.4600	41.7761	58.9031

Table 16Step response result for scenario 4 when $R_a = 0.5$ and $K_m = 0.018$.

S/ N	Algorithm- Controller	Rise time (t_r) (s)	Settling time (t_s) (s)	Max. overshoot (O_p) (%)	Steady State Error (E_{SS})
1	LHHO-PID (Proposed)	0.0387	0.0671	0.1535	4.8104e-04
2	HHO-PID [38]	0.0388	0.0672	0.1544	5.0471e-04
3	ASO-PID [35]	0.0101	0.0265	0	0.0097
4	PSO-PID [6]	0.0401	0.0685	0.3000	6.8697e-04
5	IGWO-PID [34]	0.0404	0.0685	0.3992	1.8490e-04
6	LHHO-FOPID (Proposed)	0.0212	0.0379	0	0.0012
7	HHO-FOPID [42]	0.0263	0.0518	0	0.0054
8	ASO-FOPID [4]	0.0227	0.1143	7.5417	0.0058
9	PSO-FOPID [6]	0.0229	0.1155	16.7433	0.0042
10	IGWO-FOPID [34]	0.0225	0.1147	15.8833	0.0042

the new position vector $X_{i-hawk}(new)$ among N Hawks. Then the mutation position vector $X_{i-hawk}(mut)$ for i^{th} Hawk can be modelled as given in Eq. (39).

$$X_{i-hawk}(mut) = X_{i-hawk}(new) + 2 * \left(1 - \frac{t}{t_{max}} \right) * (2 * rand - 1) (2 * X_{best-hawk}(t) - (X_{best1-hawk}(t) + X_{best2-hawk}(t))) + (2 * rand - 1) (X_{best-hawk}(t) + X_{i-hawk}(new)) \quad (39)$$

The next position vector of the Hawks $X_{i-hawk}(t+1)$ is updated using Eq. (40).

$$X_{i-hawk}(t+1) = \begin{cases} X_{i-hawk}(mut) & \text{if } fX_{i-hawk}(mut) < f(X_{i-hawk}(new)) \\ X_{i-hawk}(new) & \text{if } fX_{i-hawk}(mut) \geq f(X_{i-hawk}(new)) \end{cases} \quad (40)$$

Similarly, the vector position of the prey X_{prey} is updated using Eq. (41).

$$X_{prey} = \begin{cases} X_{i-hawk}(mut) & \text{if } fX_{i-hawk}(mut) < f(X_{prey}) \\ X_{i-hawk}(new) & \text{if } fX_{i-hawk}(mut) \geq f(X_{prey}) \end{cases} \quad (41)$$

Table 17

Frequency analysis result of the system for scenario 4 when $R_a = 0.5$ and $K_m = 0.018$.

S/ N	Algorithm- Controller	Gain margin (dB)	Phase margin (°)	Phase crossover frequency (rad/s)	Bandwidth (Hz)
1	LHHO-PID (Proposed)	Infinite	89.7288	56.0216	56.1537
2	HHO-PID [38]	Infinite	89.7268	56.0021	56.1362
3	ASO-PID [35]	Infinite	91.0762	230.4857	225.5556
4	PSO-PID [6]	Infinite	89.5613	53.7447	54.0277
5	IGWO-PID [34]	Infinite	89.4796	53.1377	53.4926
6	LHHO-FOPID (Proposed)	Infinite	90.2031	104.1723	103.7511
7	HHO-FOPID [42]	Infinite	90.1402	85.0208	84.8500
8	ASO-FOPID [4]	Infinite	75.5347	67.7208	84.3740
9	PSO-FOPID [6]	Infinite	61.5178	55.6400	79.1363
10	IGWO-FOPID [34]	Infinite	62.7536	57.3411	80.9607

Table 18

Step response result for scenario 5 when $R_a = 0.2$ and $K_m = 0.009$.

S/ N	Algorithm- Controller	Rise time (t_r) (s)	Settling time (t_s) (s)	Max. overshoot (O_p) (%)	Steady State Error (E_{SS})
1	LHHO-PID (Proposed)	0.0758	0.1261	0.6780	0.0049
2	HHO-PID [38]	0.0758	0.1261	0.6769	0.0048
3	ASO-PID [35]	0.0216	0.0512	0	0.0163
4	PSO-PID [6]	0.0780	0.1276	0.8245	0.0047
5	IGWO-PID [34]	0.0784	0.1269	0.9814	0.0057
6	LHHO-FOPID (Proposed)	0.0422	0.0740	0.1276	8.6248e-04
7	HHO-FOPID [42]	0.0542	0.1331	0	0.0065
8	ASO-FOPID [4]	0.0405	0.1629	9.0773	0.0086
9	PSO-FOPID [6]	0.0387	0.2754	19.3788	0.0064
10	IGWO-FOPID [34]	0.0381	0.2713	18.5300	0.0064

5.0. Proposed LHHO-based PID/FOPID controller

This section describes the proposed optimal parameter tuning approach based on the novel Leader Harris Hawks optimization for both PID and FOPID controllers. Since it is a popular fact that the objective function holds up a pivotal position in the determination of optimal design parameters for any controller. Over the years, numerous objective functions have been employed for tuning both integer order PID as well as fractional order PID controller design parameters. Popular among these functions include the absolute error, mean square error, as well as the integral multiplied variants (as presented in Eq. 20 to 25). In this work, we experimented with four commonly employed integral multiplied error variants, as objective function for tuning the parameters of PID and FOPID controllers. These error functions include IAE, ISE, ITAE and ITSE. Like the authors in [4,5,54], we also took ITAE as the objective function for fair comparison with other existing methods as it gives the lowest settling and rise times with reduced percentage overshoot.

The proposed LHHO algorithm was employed to identify the optimum values for the integer and fractional order parameters (K_p , K_i , K_d ,

Table 19

Frequency analysis result of the system for scenario 5 when $R_a = 0.2$ and $K_m = 0.009$.

S/ N	Algorithm- Controller	Gain margin (dB)	Phase margin (°)	Phase crossover frequency (rad/s)	Bandwidth (Hz)
1	LHHO-PID (Proposed)	Infinite	89.2438	28.0427	28.3440
2	HHO-PID [38]	Infinite	89.2399	28.0335	28.3365
3	ASO-PID [35]	Infinite	92.0973	115.1464	110.5583
4	PSO-PID [6]	Infinite	88.9141	26.9315	27.3724
5	IGWO-PID [34]	Infinite	88.7527	26.6354	27.1444
6	LHHO-FOPID (Proposed)	Infinite	90.1379	51.8460	51.6863
7	HHO-FOPID [42]	Infinite	90.6953	42.4588	41.9465
8	ASO-FOPID [4]	Infinite	71.0912	36.8762	46.8688
9	PSO-FOPID [6]	Infinite	55.6219	33.2076	47.2226
10	IGWO-FOPID [34]	Infinite	56.8909	33.9221	47.9390

Table 20

Step response result for scenario 6 when $R_a = 0.2$ and $K_m = 0.021$.

S/ N	Algorithm- Controller	Rise time (t_r) (s)	Settling time (t_s) (s)	Max. overshoot (O_p) (%)	Steady State Error (E_{SS})
1	LHHO-PID (Proposed)	0.0331	0.0569	0.2918	7.0464e-04
2	HHO-PID [38]	0.0331	0.0569	0.2918	6.8494e-04
3	ASO-PID [35]	0.0086	0.0195	0	0.0076
4	PSO-PID [6]	0.0343	0.0582	0.4352	5.4995e-04
5	IGWO-PID [34]	0.0346	0.0582	0.5254	9.6629e-04
6	LHHO-FOPID (Proposed)	0.0181	0.0323	0	3.6938e-04
7	HHO-FOPID [42]	0.0224	0.0429	0	0.0035
8	ASO-FOPID [4]	0.0197	0.1065	7.2297	0.0043
9	PSO-FOPID [6]	0.0202	0.1074	16.1851	0.0031
10	IGWO-FOPID [34]	0.0198	0.1067	15.3296	0.0031

λ and μ). The proportional, integral, and derivative parameters (K_p , K_i , K_d) are bounded within the range of 0.001–20, while the fractional powers (λ , μ) are bounded between 0 and 1 as can be seen in Table 3. During each iteration, the error value of the DC motor output is estimated and feedback into the corresponding objective function. The error values were then adjusted using the proposed LHHO algorithm as illustrated in Fig. 6. A complete system block diagram of the proposed controller employed for DC motor speed control is presented in Fig. 7.

6.0. Results and discussion

In this section, we present the simulation results of the proposed LHHO-PID and LHHO-FOPID controllers. All simulations executed in this study were conducted on MATLAB/Simulink 2022b software installed on a personal computer with an Intel (R) core i3 processor @ 3.3 GHz and 16.00 GB RAM. Specifically, the FOMCON toolbox for MATLAB was utilized due to its rich implementation and comprehensive documentation on fractional-order modeling and dynamic system control. Also, MATLAB control toolbox was also used for other control simulation and analyses. For the proposed meta-heuristics optimization

Table 21

Frequency analysis result of the system for scenario 6 when $R_a = 0.2$ and $K_m = 0.021..$

S/ N	Algorithm- Controller	Gain margin (dB)	Phase margin (°)	Phase crossover frequency (rad/s)	Bandwidth (Hz)
1	LHHO-PID (Proposed)	Infinite	89.6696	65.3511	65.5726
2	HHO-PID [38]	Infinite	89.6678	65.3283	65.5517
3	ASO-PID [35]	Infinite	90.8988	268.9014	264.0181
4	PSO-PID [6]	Infinite	89.5212	62.6888	63.0626
5	IGWO-PID [34]	Infinite	89.4498	61.9790	62.4251
6	LHHO-FOPID (Proposed)	Infinite	90.1001	121.6431	121.2869
7	HHO-FOPID [42]	Infinite	89.8968	99.2480	99.3754
8	ASO-FOPID [4]	Infinite	75.9080	78.1583	97.5548
9	PSO-FOPID [6]	Infinite	62.5019	63.0715	90.0182
10	IGWO-FOPID [34]	Infinite	63.6786	65.1287	92.2769

Table 22

Step response result for scenario 7 when $R_a = 0.6$ and $K_m = 0.009..$

S/ N	Algorithm- Controller	Rise time (t_r) (s)	Settling time (t_s) (s)	Max. overshoot (O_p) (%)	Steady State Error (E_{SS})
1	LHHO-PID (Proposed)	0.0770	0.1322	0.1814	2.9769e-04
2	HHO-PID [38]	0.0770	0.1322	0.1802	2.5243e-04
3	ASO-PID [35]	0.0218	0.0480	0	0.0191
4	PSO-PID [6]	0.0792	0.1334	0.3143	3.6097e-05
5	IGWO-PID [34]	0.0796	0.1325	0.4686	0.0011
6	LHHO-FOPID (Proposed)	0.0424	0.0756	0	0.0018
7	HHO-FOPID [42]	0.0546	0.1705	0	0.0106
8	ASO-FOPID [4]	0.0407	0.1605	8.7548	0.0113
9	PSO-FOPID [6]	0.0388	0.2800	18.9900	0.0084
10	IGWO-FOPID [34]	0.0383	0.2764	18.1574	0.0084

algorithms, the values of the parameter are as shown in [Table 3](#). To verify the efficacy and superiority of proposed controllers (LHHO-FOPID and LHHO-PID), their performance was compared not only with the baseline (HHO-FOPID and HHO-PID), but also with three other state-of-the-art meta-heuristics optimization-based controllers.

6.1. Convergence curve

In [Table 4](#), we present the quantitative comparison of the best fitness values obtained with the various objective functions considered. Based on the results presented in [Table 4](#), it can be deduced that both the proposed LHHO-FOPID controller and its PID counterpart exhibit notable advantages. They achieve a remarkably low ITSE and ITAE values while demonstrating a rapid convergence speed. With ITAE as the objective function, it is evidently shown from the results that the optimal values were obtained within the first-three (3) iterations for LHHO-FOPID controller. Also, in the case of LHHO-PID controller, the best fitness values were obtained starting from the eight (8) iteration. The convergence plot of the proposed LHHO-FOPID and LHHO-PID controllers with the baseline for 50 iterations is as shown in [Fig. 8](#).

Table 23

Frequency analysis result of the system for scenario 7 when $R_a = 0.6$ and $K_m = 0.009..$

S/ N	Algorithm- Controller	Gain margin (dB)	Phase margin (°)	Phase crossover frequency (rad/s)	Bandwidth (Hz)
1	LHHO-PID (Proposed)	Infinite	89.5466	28.0419	28.1966
2	HHO-PID [38]	Infinite	89.5428	28.0327	28.1891
3	ASO-PID [35]	Infinite	92.1717	115.1087	110.4035
4	PSO-PID [6]	Infinite	89.2294	26.9307	27.2261
5	IGWO-PID [34]	Infinite	89.0715	26.6345	26.9986
6	LHHO-FOPID (Proposed)	Infinite	90.3017	51.8456	51.6247
7	HHO-FOPID [42]	Infinite	90.8953	42.4582	41.9039
8	ASO-FOPID [4]	Infinite	71.3213	36.8757	46.7656
9	PSO-FOPID [6]	Infinite	55.8774	33.2072	47.1435
10	IGWO-FOPID [34]	Infinite	57.1410	33.9217	47.8574

Table 24

Step response result for scenario 8 when $R_a = 0.6$ and $K_m = 0.021..$

S/ N	Algorithm- Controller	Rise time (t_r) (s)	Settling time (t_s) (s)	Max. overshoot (M_p) (%)	Steady State Error (E_{SS})
1	LHHO-PID (Proposed)	0.0333	0.0582	0.0703	0.0012
2	HHO-PID [38]	0.0333	0.0582	0.0713	0.0012
3	ASO-PID [35]	0.0086	0.0199	0	0.0088
4	PSO-PID [6]	0.0345	0.0345	0.2073	0.0014
5	IGWO-PID [34]	0.0348	0.0595	0.2959	9.8854e-04
6	LHHO-FOPID (Proposed)	0.0181	0.0326	0	0.0015
7	HHO-FOPID [42]	0.0224	0.0436	0	0.0053
8	ASO-FOPID [4]	0.0198	0.1051	7.0732	0.0035
9	PSO-FOPID [6]	0.0203	0.1069	15.9879	0.0040
10	IGWO-FOPID [34]	0.0198	0.1062	15.1389	0.0040

6.2. Statistical analysis

This subsection presents the statistical analysis of LHHO algorithms and its baseline. To select optimal gain parameters for the proposed controllers, the algorithm was independently run 20 times. [Fig. 9](#) depicts the obtained best fitness values of ITAE objective function for all runs for PID and FOPID controllers. In [Table 5](#), the statistical metrics of the objective function, including parameters such as worst, best, mean, median, and standard deviation values were provided. Additionally, [Fig. 10](#) presents a boxplot illustrating these statistical measures. Analysis of both the Figures and the Table leads to the conclusion that the LHHO algorithm exhibits commendable statistical performance. Notably, even the worst score achieved by the LHHO algorithm surpasses the best outcome obtained by its baseline.

6.3. Step response analysis

In this subsection, we present the analyses of the response of the system with each of the controllers to step input. These analyses provide valuable insights to the control system dynamic characteristics, such as

Table 25

Frequency analysis result of the system for scenario 8 when $R_a = 0.6$ and $K_m = 0.021..$

S/N	Algorithm-Controller	Gain margin (dB)	Phase margin (°)	Phase crossover frequency (rad/s)	Bandwidth (Hz)
1	LHHO-PID (Proposed)	Infinite	89.7995	65.3507	65.4245
2	HHO-PID [38]	Infinite	89.7977	65.3279	65.4037
3	ASO-PID [35]	Infinite	268.9011	263.8670	263.8670
4	PSO-PID [6]	Infinite	89.6566	62.6884	62.9149
5	IGWO-PID [34]	Infinite	89.5868	61.9787	62.2777
6	LHHO-FOPID (Proposed)	Infinite	90.1699	121.6429	121.2254
7	HHO-FOPID [42]	Infinite	89.9823	99.2478	99.3328
8	ASO-FOPID [4]	Infinite	76.0166	78.1580	97.4262
9	PSO-FOPID [6]	Infinite	62.6365	63.0712	89.9140
10	IGWO-FOPID [34]	Infinite	63.8089	65.1284	92.1699

rise time, settling time, percentage overshoot, and steady-state error. It signifies how quickly the motor responds to changes in the reference signal, how accurately it reaches and maintains the desired output, as well as whether it exhibits any oscillations or overshoot. The optimal values for each tuneable parameters of the considered controllers (i.e., PID and FOPID) obtained using the proposed algorithm and other existing ones were presented in Table 6. The equivalent transfer functions for the proposed LHHO-PID and LHHO-FOPID controllers with DC motor system are as expressed in Eqs. (41) and 42, respectively.

$$G_{DC_PID}(s) = \frac{0.05039s^2 + 0.3s + 0.08156}{0.00108s^3 + 0.05649s^2 + 0.3016s + 0.08156} \quad (41)$$

$$G_{DC_FOPID}(s) = \frac{0.096204s^{1.1324} + 0.29881s^{0.13691} + 0.2987}{0.00108s^{2.1369} + 0.0061s^{1.1369} + 0.096204s^{1.1324} + 0.30044s^{0.13691} + 0.2987} \quad (42)$$

Table 7 compares the results of the step response analyses of the proposed LHHO-PID and LHHO-FOPID controllers with eight state-of-the-art controllers, namely HHO-FOPID [42], HHO-PID [38], ASO-FOPID [4], ASO-PID [35], PSO-PID [6], PSO-FOPID [6], IGWO-PID [34] and IGWO-FOPID [34]. The rise time of the proposed LHHO-PID controller and its baseline (HHO-PID) is found to be similar and second best after those obtained by ASO-PID. Among the considered PID controllers, the IGWO-PID takes the longest time to rise. Conversely, the ASO-PID controller shows the shortest duration. The proposed LHHO-FOPID controller obtained a remarkable improvement over the existing approaches, achieving a rise time of 0.0254 s. Compared to other approaches in this category, PSO-FOPID is the only controller that attained rise time close to that of proposed LHHO-FOPID controller, while other controllers such as ASO-FOPID, HHO-FOPID and IGWO-FOPID achieves 0.0265 s, 0.0318 s and 0.0260 s, respectively.

With respect to settling time, the proposed LHHO-PID controller attain roughly the same value as its baselines, settling at 0.0794 s and 0.0795 s time duration, respectively. In addition, PSO-PID and IGWO-PID controllers also took 0.0809 s and 0.0808 s, respectively, while ASO-PID controller took 0.0835 s been the longest settling time among all controllers in this category. The proposed LHHO-FOPID took 0.0453 s to settle which is the lowest among other benchmark controllers in the category. Compared with the baseline (HHO-FOPID) and PSO-FOPID controllers which took 0.0641 s, 0.1267s, ASO-FOPID and IGWO-FOPID controllers settles almost at the same time of 0.1258s and 0.1257s respectively. Thus, the proposed controller in this category contributes an improvement of about 29.33 % to 63.96 % relative to the state-of-the-arts.

In terms of maximum overshoot, ASO-PID is the only controller without overshoot while the performance obtained by the proposed LHHO-PID controller, and its baseline compared to others remain the most competitive after ASO-PID. Likewise, in the FOPID category, PSO-

FOPID controller attained the highest maximum overshoot with a value of 17.5882 %, translating to the worst performance in term of this metric. The performance of IGWO-FOPID and ASO-FOPID controllers are similar to PSO-FOPID achieving a maximum overshoot of 16.7203 % and 8.0645 %, respectively. However, the performance obtained by the proposed LHHO-FOPID controller, and the baseline are the most competitive in this category, with HHO-FOPID attaining zero overshoot while LHHO-FOPID achieved 0.0456 %. The steady state error obtained by the proposed controllers are closer to zero compared to others as seen in Table 7. Figs. 11 and 12 provide a comprehensive comparison of the step response among the state-of-the-art controllers and the proposed LHHO-PID and LHHO-FOPID controllers. These figures offer enhanced

visualizations to Table 7 to facilitate detailed analysis of the performance differences. As seen from these figures, the proposed controllers have better performance not just to the baseline [38] and [42], but also to other state-of-the-art controllers such as ASO [4], PSO [6], and IGWO [34], attaining minimum overshoot, and reduced settling and rise time.

6.4. Frequency response analysis

This subsection describes the frequency response of the system under consideration in terms of gain margin, phase margin and bandwidth. This analysis provides a valuable insight into the system stability characteristics. While the gain margin quantifies the amplification or attenuation of the input, the phase margin measures the time delay between the input and output signals. Moreover, the bandwidth represents the frequency range over which the DC motor-controlled system operates effectively. Figs. 13 and 14 present the bode plots of the proposed controllers and its baselines. The comparison of the frequency response analysis for the proposed controllers and other existing ones are shown in Table 8. All controllers including the proposed attained infinite gain margin. However, in terms of phase margin, ASO-PID attain the best with a value of 91.2804°. Similarly, in the FOPID category, the proposed LHHO-FOPID controller and its baseline outperforms the state-of-the-art by obtaining approximately equal phase margin. The bandwidth value attained by the ASO-PID is the best among other controllers in PID category, followed by the proposed LHHO-PID controller with bandwidth of 46.8832 Hz. Similarly, the best value of bandwidth attained by controllers in FOPID category is attained by the proposed LHHO-FOPID controller with the value of 86.3234 Hz. Furthermore, the phase crossing frequency of the proposed controllers are excellent, with LHHO-PID and LHHO-FOPID attaining 46.6933 rad/s and 86.7057 rad/s, respectively.

2.5. Robustness analysis

The presence of a robust controller is crucial for maintaining an acceptable system response during abnormal scenarios. To evaluate the behavior of the system under different conditions, robustness analysis was performed under load variations. In the proposed method, the robustness analysis involved altering the armature resistance (R_a) and the torque constant (K_m) of the DC motor by $\pm 25\%$ and $\pm 20\%$, and $\pm 50\%$ and $\pm 40\%$ respectively, resulting in eight distinct scenarios as outlined in Table 9.

To assess the efficiency of the system under the various scenarios, several experiments were conducted, and step and frequency responses were observed. The obtained results revealed that the proposed controllers are highly robust to mild, severe, and normal load variations, as can be seen in Tables 10–25. It is evident from a close examination of the presented tables that the proposed controllers consistently exhibit the best performance for both step and frequency response analyses. The findings confirm the robustness of the proposed controllers for speed control, as it successfully maintains desirable performance despite changes in DC motor system parameters.

7.0. Conclusion

The complexity of various industrial control processes in recent years have necessitate the need for an optimal and robust controller parameter tuning algorithm. In this respect, a novel LHHO meta-heuristic-based algorithm was reported in this study. As an improvement to the baseline (HHO), this work exploits the leadership prowess and adaptive perching strategy of the hawks to select the best parameters for the controllers. The proposed controllers were successfully applied to DC motor speed regulation. To obtain the best design parameters, and thus desired system response, the controllers proposed in this study were experimented with four different error functions namely IAE, ISE, ITSE, and ITAE. Among all, as also reported in previous studies, this study found that ITAE gives the best performance. During evaluation, the proposed controllers were not only compared with the baseline (HHO-PID/FOPID), but also with state-of-the-art algorithms including PSO-PID/FOPID, ASO-PID/FOPID, and IGWO-PID/FOPID. A quantitative comparison of time response analysis with the state-of-the-art revealed that the proposed LHHO-FOPID controller contributes 4.15 %, 29.33 %, 99.43 % and 87.68 % improvement in rise time, settling time, maximum overshoot, and steady state error respectively. While the stability response and robustness analyses of the proposed controllers also indicate a competitive performance, its robustness to load disturbance and/or rapidly varying motors parameters like motor's back electromotive force, armature resistance, etc., is still open to further improvement. In the future, the proposed controller tuning approach can be applied to a more complex control system including cascade and fuzzy logic-based controllers as well as highly varying disturbances. Moreover, other objective functions such as Zwe-Lee Gaing (ZLG) and its variants can also be investigated on the proposed method.

Declaration of Competing Interest

The authors declare that they have no known competing financial interests or personal relationships that could have appeared to influence the work reported in this paper.

References

- [1] N. Thomas, D.P. Poongodi, Position control of DC motor using genetic algorithm based PID controller, in: Proceedings of the world congress on engineering 2, Citeseer, 2009, pp. 1–3.
- [2] M. Ruderman, J. Krettek, F. Hoffmann, T. Bertram, Optimal state space control of DC motor, IFAC Proceed. 41 (2) (2008) 5796–5801.
- [3] B.A. Reddy, D. Sowjanya, Control of DC motor using sliding mode control under disturbance conditions, in: 2019 Third International Conference on Inventive Systems and Control (ICISC), IEEE, 2019, pp. 32–36.
- [4] B. Hekimoğlu, Optimal tuning of fractional order PID controller for DC motor speed control via chaotic atom search optimization algorithm, IEEE Access 7 (2019) 38100–38114.
- [5] S. Ekinci, B. Hekimoğlu, D. Izci, Opposition based Henry gas solubility optimization as a novel algorithm for PID control of DC motor, Eng. Sci. Technol., Int. J. 24 (2) (2021) 331–342.
- [6] Z. Qi, Q. Shi, H. Zhang, Tuning of digital PID controllers using particle swarm optimization algorithm for a CAN-based DC motor subject to stochastic delays, IEEE Trans. Ind. Electron. 67 (7) (2019) 5637–5646.
- [7] J.M. Diaz, R. Costa-Castello, S. Dormido, Closed-loop shaping linear control system design: an interactive teaching/learning approach [focus on education], IEEE Contr. Syst. Mag. 39 (5) (2019) 58–74.
- [8] S.B. Joseph, E.G. Dada, A. Abidemi, D.O. Oyewola, B.M. Khammas, Metaheuristic algorithms for PID controller parameters tuning: review, approaches and open problems, Heliyon 8 (5) (2022) e09399, <https://doi.org/10.1016/j.heliyon.2022.e09399>, 2022/05/01.
- [9] R.P. Borase, D. Maghade, S. Sonkar, S. Pawar, A review of PID control, tuning methods and applications, Int. J. Dyn. Control 9 (2021) 818–827.
- [10] S. Bharat, A. Ganguly, R. Chatterjee, B. Basak, D.K. Sheet, A. Ganguly, A review on tuning methods for PID controller, Asian J. Converg. Technol. (AJCT) (2019). ISSN-2350-1146.
- [11] D. Sain, S.K. Swain, S.K. Mishra, TID and I-TD controller design for magnetic levitation system using genetic algorithm, Perspect. Sci. 8 (2016) 370–373.
- [12] B.J. Lurie, "Three-parameter tunable tilt-integral-derivative (TID) controller," 1994.
- [13] I. Podlubny, Fractional-order systems and PI/ $\sup/\text{spl lambda}/D/\sup/\text{spl mu}/$ -controllers, IEEE Trans. Automat. Contr. 44 (1) (1999) 208–214.
- [14] S. Das, Functional Fractional Calculus, Springer, 2011.
- [15] J. Munoz, C.A. Monje, L.F. Nagua, C. Balaguer, A graphical tuning method for fractional order controllers based on iso-slope phase curves, ISA Trans. 105 (2020) 296–307.
- [16] J. Agarwal, G. Parmar, R. Gupta, A. Sikander, Analysis of grey wolf optimizer based fractional order PID controller in speed control of DC motor, Microsyst. Technol. 24 (2018) 4997–5006.
- [17] S. Das, S. Saha, S. Das, A. Gupta, On the selection of tuning methodology of FOPID controllers for the control of higher order processes, ISA Trans. 50 (3) (2011) 376–388, <https://doi.org/10.1016/j.isatra.2011.02.003>.
- [18] D. Valerio, J.S. da Costa, A review of tuning methods for fractional PIDs, in: 4th IFAC Workshop on Fractional Differentiation and its Applications 10, FDA, 2010 no. 5.
- [19] P. Shah, S. Agashe, Review of fractional PID controller, Mechatronics 38 (2016) 29–41, <https://doi.org/10.1016/j.mechatronics.2016.06.005>.
- [20] V. Kumar, V. Sharma, R. Naresh, Leader Harris Hawks algorithm based optimal controller for automatic generation control in PV-hydro-wind integrated power network, Electr. Power Syst. Res. 214 (2023), 108924.
- [21] B. Su, Y. Lin, J. Wang, X. Quan, Z. Chang, C. Rui, Sewage treatment system for improving energy efficiency based on particle swarm optimization algorithm, Energy Rep. 8 (2022) 8701–8708.
- [22] J.-S. Pan, J.-X. Lv, L.-J. Yan, S.-W. Weng, S.-C. Chu, J.-K. Xue, Golden eagle optimizer with double learning strategies for 3D path planning of UAV in power inspection, Math. Comput. Simul. 193 (2022) 509–532.
- [23] J.R. Nayak, B. Shaw, B.K. Sahu, K.A. Naidu, Application of optimized adaptive crow search algorithm based two degree of freedom optimal fuzzy PID controller for AGC system, Eng. Sci. Technol., Int. J. 32 (2022), 101061.
- [24] D. Izci, S. Ekinci, S. Mirjalili, L. Abualigah, An intelligent tuning scheme with a master/slave approach for efficient control of the automatic voltage regulator, Neural Computing and Applications, 2023, pp. 1–17.
- [25] D. Izci, S. Ekinci, E. Eker, A. Demiroren, Biomedical application of a random learning and elite opposition-based weighted mean of vectors algorithm with pattern search mechanism, J. Control., Automat. Electr. Syst. 34 (2) (2023) 333–343.
- [26] Y. Wang, Y. Xiao, Y. Guo, J. Li, Dynamic chaotic opposition-based learning-driven hybrid aquila optimizer and artificial rabbits optimization algorithm: framework and applications, Processes 10 (12) (2022) 2703.
- [27] Y. Xiao, Y. Guo, H. Cui, Y. Wang, J. Li, Y. Zhang, IHAAVOA: an improved hybrid aquila optimizer and African vultures optimization algorithm for global optimization problems, Math. Biosci. Eng. 19 (11) (2022) 10963–11017.
- [28] Y. Xiao, X. Sun, Y. Guo, S. Li, Y. Zhang, Y. Wang, An improved gorilla troops optimizer based on lens opposition-based learning and adaptive β -hill climbing for global optimization, Cmes-Comput. Model. Eng. Sci. 131 (2) (2022).
- [29] T. Amieur, D. Taibi, S. Kahla, M. Bechouat, M. Sedraoui, Tilt-fractional order proportional integral derivative control for DC motor using particle swarm optimization, Electr. Eng. Electromech. (2) (2023) 14–19.
- [30] P. Dutta, S.K. Nayak, Grey wolf optimizer based PID controller for speed control of BLDC motor, J. Electr. Eng. Technol. 16 (2021) 955–961.
- [31] M.A. Ibrahim, A.K. Mahmood, N.S. Sultan, Optimal PID controller of a brushless DC motor using genetic algorithm, Int. J. Pow. Elec. Dri. Syst. ISSN 2088 (8694) (2019) 8694.
- [32] M. Misagh, M. Yaghoobi, Improved invasive weed optimization algorithm (IWO) based on chaos theory for optimal design of PID controller, J. Comput. Des. Eng. 6 (3) (2019) 284–295.
- [33] R. Saini, G. Parmar, R. Gupta, SFS based fractional order PID controller (FOPID) for speed control of DC motor, Int. J. 9 (4) (2020).

- [34] L.-L. Li, J.-Q. Liu, W.-B. Zhao, L. Dong, Fault diagnosis of high-speed brushless permanent-magnet DC motor based on support vector machine optimized by modified grey wolf optimization algorithm, *Symmetry (Basel)* 13 (2) (2021) 163.
- [35] E. Eker, M. Kayri, S. Ekinci, D. Izci, A new fusion of ASO with SA algorithm and its applications to MLP training and DC motor speed control, *Arab. J. Sci. Eng.* 46 (2021) 3889–3911.
- [36] D. Izci, S. Ekinci, H.L. Zeynelgil, J. Hedley, Performance evaluation of a novel improved slime mould algorithm for direct current motor and automatic voltage regulator systems, *Trans. Inst. Meas. Control* 44 (2) (2022) 435–456.
- [37] D. Izci, S. Ekinci, H.L. Zeynelgil, J. Hedley, Fractional order PID design based on novel improved slime mould algorithm, *Electr. Power Compon. Syst.* 49 (9–10) (2021) 901–918.
- [38] S. Ekinci, D. Izci, B. Hekimoğlu, PID speed control of DC motor using Harris Hawks optimization algorithm, in: 2020 International conference on electrical, communication, and computer engineering (ICECCE), IEEE, 2020, pp. 1–6.
- [39] M. Khalilpour, N. Razmjooy, H. Hosseini, P. Moallem, Optimal control of DC motor using invasive weed optimization (IWO) algorithm, in: Majlesi Conference on Electrical Engineering, Majlesi New Town, Isfahan, Iran, 2011.
- [40] I. Khanam, G. Parmar, Application of SFS algorithm in control of DC motor and comparative analysis, in: 2017 4th IEEE Uttar Pradesh Section International Conference on Electrical, Computer and Electronics (UPCON), IEEE, 2017, pp. 256–261.
- [41] A.A. Heidari, S. Mirjalili, H. Faris, I. Aljarah, M. Mafarja, H. Chen, Harris hawks optimization: algorithm and applications, *Future Generat. Comput. Syst.* 97 (2019) 849–872, <https://doi.org/10.1016/j.future.2019.02.028>, 2019/08/01/.
- [42] V.K. Munagala, R.K. Jatoh, Design of fractional-order PID/PID controller for speed control of DC motor using Harris Hawks optimization, *Intell. algor. anal. contr. dyn. syst.* (2021) 103–113.
- [43] V.K. Munagala, R.K. Jatoh, A novel approach for controlling DC motor speed using NARXnet based FOPID controller, *Evol. Syst.* 14 (1) (2023) 101–116.
- [44] M.K. Naik, R. Panda, A. Wunnava, B. Jena, A. Abraham, A leader Harris Hawks optimization for 2-D Masi entropy-based multilevel image thresholding, *Multimedia Tools and Applications*, 2021, pp. 1–41.
- [45] B. Hekimoğlu, S. Ekinci, V. Demiray, R. Dogurucu, A. Yıldırım, Speed control of DC motor using PID controller tuned by salp swarm algorithm, in: Proc. IENSC, 2018, pp. 1878–1889.
- [46] K. Ogata, *System Dynamics*, Pearson Education, Inc., Englewood Cliffs, NJ, USA, 2004, p. 768.
- [47] S. Ekinci, D. Izci, B. Hekimoğlu, Optimal FOPID speed control of DC motor via opposition-based hybrid manta ray foraging optimization and simulated annealing algorithm, *Arab. J. Sci. Eng.* 46 (2) (2021) 1395–1409.
- [48] D. Izci, S. Ekinci, Comparative performance analysis of slime mould algorithm for efficient design of proportional-integral-derivative controller, *Electrica* 21 (1) (2021).
- [49] D. Izci, Design and application of an optimally tuned PID controller for DC motor speed regulation via a novel hybrid Lévy flight distribution and Nelder-Mead algorithm, *Trans. Inst. Meas. Control* 43 (14) (2021) 3195–3211.
- [50] S. Ekinci, B. Hekimoğlu, A. Demirören, E. Eker, Speed control of DC motor using improved sine cosine algorithm based PID controller, in: 2019 3rd International Symposium on Multidisciplinary Studies and Innovative Technologies (ISMSIT), IEEE, 2019, pp. 1–7.
- [51] S. Baru, S. Gupta, A. Shukla, Comparative study of controller scheme and tuning methods, in: 2022 1st International Conference on Sustainable Technology for Power and Energy Systems (STPES), IEEE, 2022, pp. 1–6.
- [52] R. Kumar, V. Singh, A. Mathur, *Intelligent Algorithms for Analysis and Control of Dynamical Systems*, Springer, 2021.
- [53] X.-S. Yang, *Nature-inspired Metaheuristic Algorithms*, Luniver press, 2010.
- [54] A. Ajiboye, J. Popoola, O. Onyiide, S. Ayinla, PID controller for microsatellite yaw-axis attitude control system using ITAE method, *TELKOMNIKA (Telecommun. Comput. Electr. Control)* 18 (2) (2020) 1001–1011.